Optical and Quantum Electronics (2023) 55:1105
https://doi.org/10.1007/s11082-023-05432-1

Centrosymmetric crystal structure and third order nonlinear optical properties of $[2(C_{10}H_{20}O_5) NH_4] [Cd (SCN)_3]$: CCTC single crystal for optical application

S. Ramkumar[1] · P. Malliga[1]

Received: 28 March 2023 / Accepted: 14 September 2023 / Published online: 29 September 2023

Abstract
A novel Bis-15-crown-5-ether cadmium tri-thiocyanate non-linear optical single crystal was synthesized by the slow evaporation method. The single crystal X-ray diffraction pattern was utilized to determine the crystal structure, lattice parameters and symmetry. It reveals the grown title compound is monoclinic structure and underwent a centrosymmetric space group of $P2_{1/n}$. The prepared sample functional groups and optical properties were analyzed by FTIR, micro Raman and UV–Vis-NIR spectrum. The sample optical cut-off wavelength was found in the deep UV region and the band gap was calculated from Tauc's relation. Additionally, crystal growth mechanisms such as surface morphology, reverse growth rate and elemental composition were observed from the high-resolution-scanning electron microscope, etching and energy dispersive spectroscopy studies. Moreover, thermal and mechanical stability were examined by TG–DTA, Vickers hardness studies. At room temperature, the as-grown crystal dielectric constant (ε_r) and dielectric loss (tanδ) were studied as a function of temperature and the results are discussed. The third-order non-linear optical properties were obtained from Z-scan studies under 633 nm excitation.

Keywords Centrosymmetric structure · Mechanical strength · Thermal stability · Z-scan studies

1 Introduction

In recent years, materials with enhanced growth of organometallic thiocyanate complex systems formed by inorganic polymers and organic spacers (IPOS) of single crystal with unique properties have been used in nonlinear optical (NLO) applications for optical bi-stable devices, frequency doubling, tripling conversion, optical switching, photonics, optoelectronics and optical communications (Vijayalakshmi et al. 2016; Mahendiran

✉ P. Malliga
calltomp@gmail.com

S. Ramkumar
ramkumar2118@gmail.com

[1] Department of Physics, Sathyabama Institute of Science and Technology, Chennai, Tamil Nadu 600 119, India

et al. 2016; Yuanet et al.1988). Even though many organic and inorganic composites exist, an optical frequency conversion is achieved to increase NLO efficiency (Kamalesh et al. 2020; Senthil et al. 2014; Karuppasamy et al. 2016). In this way, coordination complexes intermingle the advantages of organic and inorganic materials that can exist in the crystalline structure. Moreover, the physiochemical properties of the IPOS complex are achieved by various measurements such as moderate solubility, thermal stability, mechanical and high-order NLO properties (Ferdaousse Rhoufal et al. 2019; Vinay Paroll et al.2020).

According to double ligand theory, the organometallic structure that contains a unique charge transfer from metal to linkers or linkers to metal complexes was transferred. The formula of IPOS is AB $(SCN)_4$, in this case, AB = divalent metal ion, ligand = SCN^- forming a 3D structure. The structural modification of IPOS designed by the hard-soft-acid–base concept. For this process, the heteroatoms like S, and N played as acceptors, which always bind with the ligand. Even though SCN^- is a thiocyanate, it makes good coordination compounds with Cd^{2+}, Zn^{2+}, Mn^{2+} and Hg^{2+}. As per the above mentioned formula, both transition metals (AB) and ligands (SCN^-) are major backbone formations of IPOS, also structure of the skeleton indicates a centrosymmetric space group, this is because of d-d transitions with low energy.

The preparation of a stable complex is always a major concern which can be accomplished by choosing host materials (crown ether) and guest (metal complexes). These approaches depend on cavity diameter and cation size because these prepared materials are closely packed. Many kinds of crown ether atomic models are available, and this diameter of 15-Crown-5 ether ($C_{10}H_{20}O_5$) 1.7 to 2.2 Å (Ravisankar et al. 2021a, b, c). In this context, novel organometallic thiocyanate $[2(C_{10}H_{20}O_5)\ NH_4]\ [Cd\ (SCN_3)]$: CCTC crystal originated from metal ions Cd (0.95 Å) were bonded to SCN of the sulphur site, NH_4 combined with 15-Crown-5 ether and formed the new crystalline arrangement of CCTC (Cliffe and Keyzer et al. 2019; Saravana et al. 2018). The majority of organometallic thiocyanate family crystals are synthesized by using the slow evaporation solution growth technique (SESGT). The grown CCTC crystal are performed by single crystal-XRD (SXRD), Fourier transform infrared (FT-IR), micro-Raman spectroscopy, UV–Vis-NIR spectrum, thermal stability (TG/DTA), Vickers micro-hardness and chemical etching studies. Additionally, High resolution (HR) scanning electron microscopy (SEM) with energy dispersive spectroscopy (EDS), CHNS and dielectric studies results are discussed. The third-order NLO properties were measured by Z-scan studies.

2 Experimental procedure

2.1 Materials

All the precursor materials were used in AR-grade cadmium chloride ($CdCl_2$), 15-crown-5 ether ($C_{10}H_{20}O_5$) and ammonium thiocyanate (NH_4SCN). Solvents such as water, methanol and ethanol. The resulting chemical scheme (Fig. 1) and synthesis reaction as follows:

$$CdCl_2 + 2\left(C_{10}H_{20}O_5\right) + 3\left[NH_4SCN\right] \rightarrow \left[NH_4\left(C_{10}H_{20}O_5\right)_2\right] \cdot \left[Cd\ (SCN)_3\right] + 2NH_4Cl$$

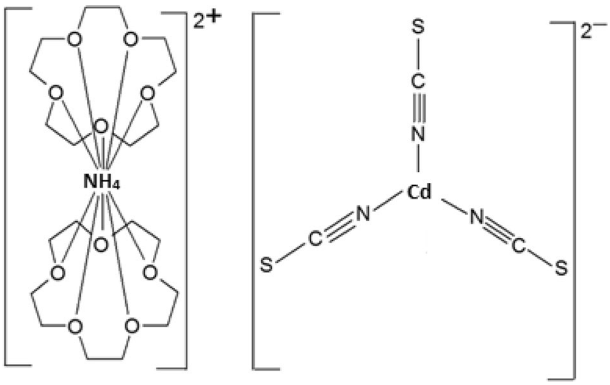

Fig. 1 Chemical scheme of CCTC single-crystal

2.1.1 Synthesis and crystal growth

The starting materials of $CdCl_2$, NH_4SCN and crown ether were taken in different beaker. The three chemical compounds were dissolved in mixture solvents of water, methanol, 1, 2-dichloroethane (2:2:1 ratio) and stirred for one hour. All these three solutions mixed together and small amount of white precipitate settled at the bottom of the beaker. To avoid this, the reaction product was gently heated above room temperature to increase the solubility of the solution. Then the solutions was continuously stirred for 8 h. Finally the clear saturated homogeneous solution was filtered with whatman 125 mm grade paper also kept in a sealed container for crystallization without further disturbances. The grown crystalline blocks were harvested over a period of 20–25 days and they possess seed crystal dimensions of $10 \times 3 \times 2$ mm^3 as shown in Fig. 2. To ensure purity, recrystallization was carried out twice.

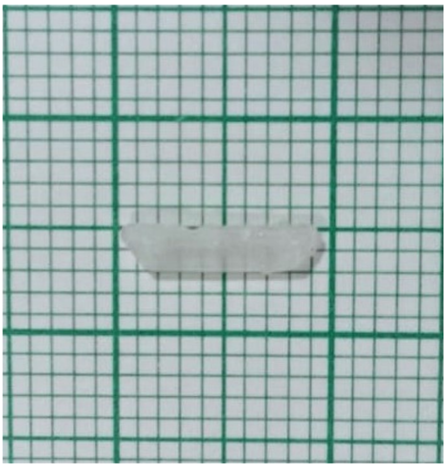

Fig. 2 Photograph of CCTC single-crystal

2.1.2 Solubility measurement

Solubility tests are an essential factor for growing single crystals. The solubility of the grown CCTC crystal was plotted between solubility of the solute with respect to temperature (35 to 50 °C) as shown in Fig. 3. The solubility curve reveals that, compared to water, moderately better soluble in methanol. The CCTC has low solubility in water but is conveniently soluble in methanol although it is little crucial to grow in bulk at environmental temperature. Therefore, a mixture compound (water: methanol: 1, 2-dichloroethane) taken in the ratio of 2:2:1 was optimized after several attempts in order to synthesize a grown CCTC crystal.

3 Result and discussions

3.1 Structural studies: single crystal X-ray diffraction

As-grown CCTC structure were investigated by using a Bruker-Kappa APEX II CCD diffractometer and Molybdenum Kα (0.7107 Å) radiation and scanning mode ω/2θ. The cell refinement and data reduction can be determined by using SAINT (Bruker APEX2 2008). A cumulative value of unique reflections was observed in 133,609, out of 6422 individual reflections (I > 2σ (I)) and 382 variable of parameters. With SADABS (Sheldrick 1996), the intensities for Lorentz, polarization effects and absorption corrections were fixed. The CCTC structure was solved by a direct method for this procedure employed on SHELXS97 (Sheldrick 2008), refined by SHELXL 2018. Non-hydrogen (H) atoms obscure the significant role of positions using the full-matrix least-squares technique; the reliability (R) factor was 0.0828. The title compound CCTC exhibits a monoclinic structure, also under centrosymmetric space group $P2_{1/n}$. The CCTC lattice dimensions are $a = 13.891$ (5) Å, $b = 10.773$ (4) Å, $c = 23.157$ (11) Å, $\alpha = \gamma = 90°$, $\beta = 91.763(2)$ ° and volume (V) = 3464.3(2) Å^3. Crystallographic details and the refinements of the grown CCTC crystal are described in Table 1. The ORTEP plot of the title molecule at an ellipsoid level

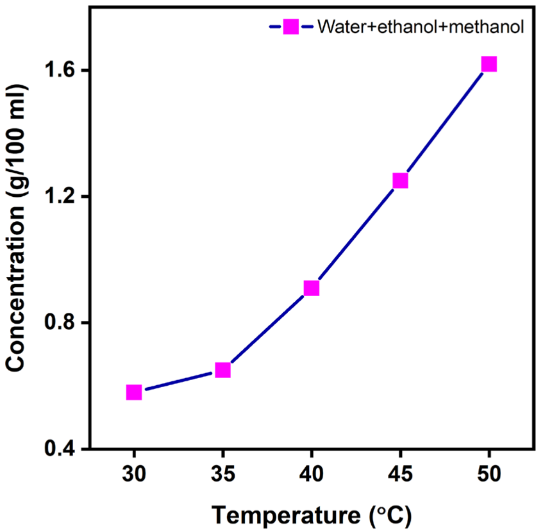

Fig. 3 Solubility curve of CCTC

Table 1 Crystal data, data collection and structure refinement

Identification Code	SHELX
Chemical formula	$C_{23}H_{44}CdN_4O_{10}S_3$
Formula weight	745.20
Crystal system, space-group	Monoclinic, $P2_1/n$
Cell dimensions	$a = 13.891(5)$Å, $b = 10.773(4)$Å $c = 23.157(11)$ Å: $\alpha = \gamma = 90°$, $\beta = 91.763(2)°$
T (K)	296(2)
λ (Å)	0.71073
V (Å^{3})	3464.3(2)
D_x (g /cm^3)	1.429
Z	4
hkl ranges	$-16 <= h <= 16, -13 <= k <= 13, -28 <= l <= 28$
Θ range (°)	1.56–26.61
No. of parameters	382
Goodness of fit	1.123
R (F) [I > 2σ (I)]	0.0828
R (F) (all data)	0.0947
Max/min Δρ (e.Å^{-3})	1.079 and -0.826

of 30% probability is shown in Fig. 4a. In CCTC, Cd^{II} ions, SCN^- ligands are both placed in the same plane whereas 15-crown-5-ether ammonium ions (NH_4) are located on the mirror plane. It results in a chain-like arrangement. In an asymmetric unit, one half has cations and the other contains anions. In this structure three N atoms are attached to Cd^{II} ions and ten O atoms, two 15-crown-5 ether ligands under and above connected with NH_4 and its sandwich configuration shown in Fig. 4b (Ravisankar et al. 2021a, 2021b, 2021c). The Hydrogen bond data details are listed in Table 2.

3.2 UV–Visible-NIR spectral studies

The optical properties of the grown CCTC crystal depends on optical absorbance, transmittance, band gap (E_g) and optical absorption coefficient (α). SHIMADZU UV 3600 PLUS instrument can be used to describe grown crystals in the 200–2000 nm range. Absorption and transmittance spectra of the grown CCTC crystal results are shown in Fig. 5a and b. As seen in the transmittance spectrum, the sample cut-off wavelength was found to be 271 nm. The material shows higher transmittance in the visible and near infrared region, so we concluded the grown crystal is applicable for NLO device applications (Johnson et al. 2018). The UV cut-off wavelength of CCTC is less than other thiocyanate family materials such as CMTC (371 nm), LATC (320 nm) (Tejaswi Ashok Hegde et al. 2018; Suresh et al. 2018). The sample has a wide optical window of 400–2000 nm and a very low absorption value over a wide range of optical transparency in the visible and NIR regions. Cd^{2+} ion broad peak seen in both absorption and transmittance spectra in the NIR region near 1200 nm. The absorption coefficient (α) was studied using the formula (Raghavan et al. 2010)

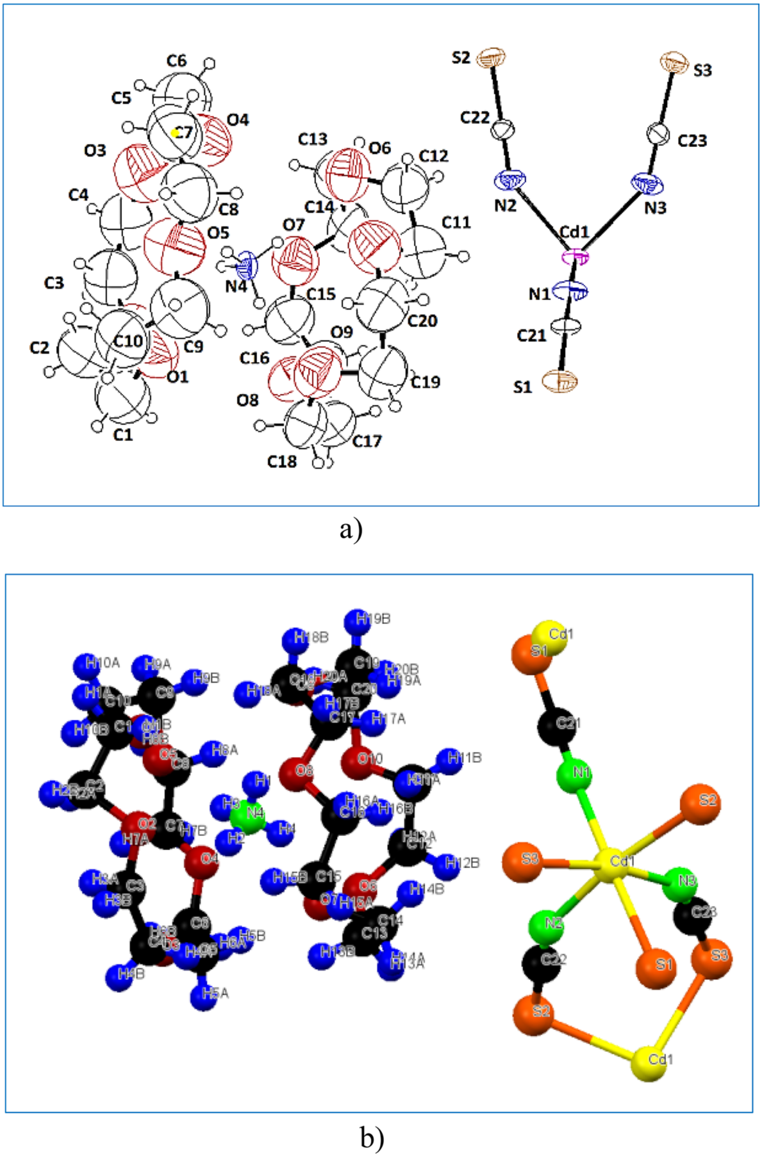

Fig. 4 **a** ORTEP plot of the molecule with atom numbering scheme drawn at 30% probability ellipsoid level. **b** Molecular structure of CCTC

$$\alpha = \frac{2.3026}{t}\left(\frac{100}{T}\right) \tag{1}$$

Here T = optical transmittance (%) and t = thickness of the material (mm).

Band gap (E_g) can be experimentally estimated using dependence of the absorption coefficient (α) on photon energy.

Table 2 Hydrogen bond data and angle (Å and °) of the compound

D-H…A	D-H	H…A	D…A	DHA
C(7)-H(7B)…N(1)^3	0.97	2.54	3.41(3)	149.5
C(2)-H(2B)…S(1)^4	0.97	2.97	3.82(3)	147.1
C(4)-H(4B)…N(3)^4	0.97	2.62	3.53(3)	155.2
N(4)-H(2)…O(2)	0.858(17)	2.49(5)	3.11(2)	131(5)
N(4)-H(1)…O(8)	0.857(17)	2.38(5)	2.998(16)	129(5)
N(4)-H(1)…O(9)	0.857(17)	2.26(4)	3.037(18)	150(5)
N(4)-H(4)…O(6)	0.851(18)	2.24(3)	3.084(19)	172(5)
N(4)-H(4)…O(10)	0.851(18)	2.57(6)	3.057(19)	117(5)
N(4)-H(3)…O(4)	0.858(17)	2.51(5)	3.14(2)	131(5)
N(4)-H(3)…O(5)	0.858(17)	2.15(3)	2.98(2)	162(6)

Symmetry operators: (i) − x + 3/2, y − 1/2,-z + 1/2 (ii) − x + 3/2, y + 1/2, − z + 1/2 (iii) − x + 1, − y + 1, − z + 1 (iv) x − 1,y,z

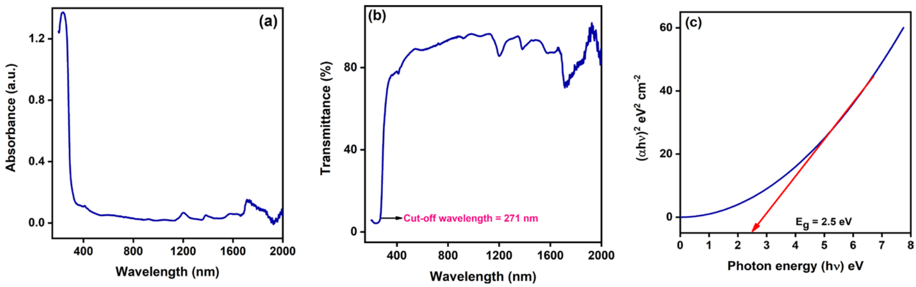

Fig. 5 UV–Vis-NIR **a** absorbance **b** transmittance and **c** band gap (Tauc's plot) of CCTC

$$\alpha h\gamma = A\left(h\gamma - E_g\right)^2 \quad (2)$$

where 'h' Planck's constant (6.626×10^{-34} J/s) and 'E_g' bandgap is deduced by extrapolating line segment ratio of $(\alpha h\gamma)^2$, photon energy (hγ) which is shown in Fig. 5c. The direct bandgap of the as-prepared sample observed value 2.5 eV. The CCTC crystal band gap revealed better optical quality compared with other materials like CMTC (2.04 eV), MCCTC (1.70 eV) (Ramesh et al. 2012; Robert et al. 2010). The CCTC possesses UV cut-off wavelength and band gap values competent for optical applications.

3.3 Vibrational spectroscopy studies

FT-IR is a useful tool to investigate the presence of molecular vibration and functional groups. The title compound chemical bond was observed by using BRUKER IFS66V FTIR instrument operating in ATR mode (400—4000 cm^{-1}). The recorded IR and Raman spectra are displayed in Fig. 6a and b. The strong absorption peak observed at 2064 cm^{-1} characteristic peak emphasized by the CN stretching thiocyanate ligand SCN^- (Rajarajan et al. 2013). The bending vibrations of δ (SCN^-) and 2δ (SCN^-) occur at 468 and 821 cm^{-1} which confirm the metal-nitrogen (Cd–N) and metal sulphur compound presented in CCTC

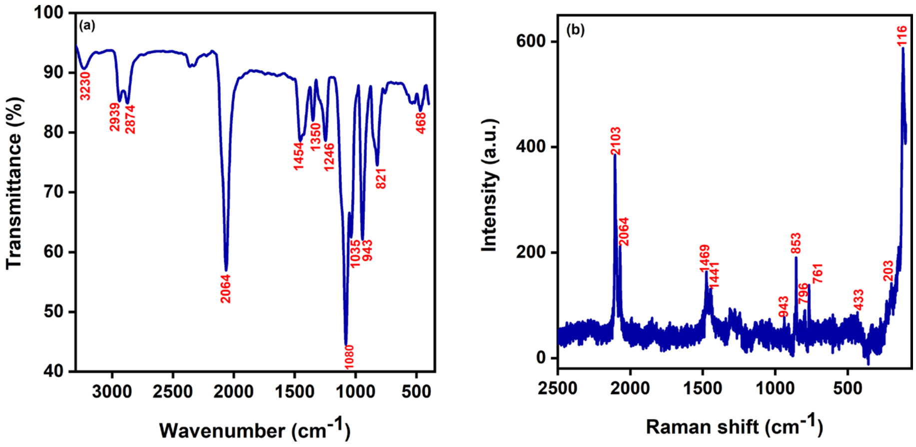

Fig. 6 **a** FT-IR **b** Micro-Raman spectrum of CCTC

(Ravisankar et al. 2022). Earlier, as reported by bending and stretching vibrations of the Cd-Cl bonds which possess two sharp and low intensity peaks at 2874, 2939 cm^{-1}, respectively (Ramesh et al. 2013). A peak position at 1350 cm^{-1} was observed and called as C-H rock vibrations. Furthermore, three peaks are found in the scale of FT-IR spectrum at 943, 1035 and 1080 cm^{-1} these can be ascribed as =C–H bending, =C–O–C asymmetric and symmetric stretching vibrations. In addition, the micro-Raman spectrum of CCTC crystal was recorded from 50 to 4000 cm^{-1} at room temperature. From the results, Cd metal ions are responsible for bending vibrational bands at 203 and 116 cm^{-1}. The presence of sharp CN stretching SCN^- ligand has extremely influenced the strong peak observed at 2064 cm^{-1}. The IR and Raman spectral studies results are listed in Table 3.

3.4 HR-SEM and EDS mapping

Surface morphology, structural features of as-prepared grown crystals were examined by HR-SEM analysis. Using the HITACHI S4800 instrument, images were taken with a low accelerated voltage (10 kV), the crystal was kept in a high vacuum with a viewing field of 20 µm. The scanning electron microscope (SEM) image of the CCTC crystal at different magnifications is displayed in Fig. 7a, b and c. The crack-free nature of the

Table 3 FT-IR and micro-Raman spectral assignments of CCTC

Wave Number (cm^{-1})		Band assignments
IR	Raman	
2874 and 2939	–	Bending and stretching vibrations of the Cd-Cl bonds
2064	2064	CN-stretching vibration of SCN (thiocyanate)
1350	–	C-H rock vibration
1035 and 1080	–	=C–O–C asymmetric and symmetric stretching vibration
943	–	=C–H bend
468 and 821	–	Metal-Nitrogen stretch

surface at 1 μm and randomly oriented needle shaped structures of 2 μm and 500 nm are observed. Elemental composition of CCTC material established by EDS spectrum. From the results of EDS (Fig. 8), cadmium (Cd), chlorine (Cl) and thiocyanate ligand (SCN^-) presented in the title compound. The experimental data agree with the theoretical values listed in Table 4.

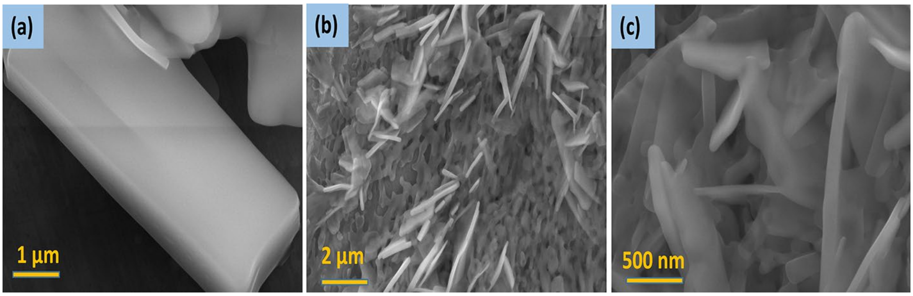

Fig. 7 **a**, **b** and **c** HR-SEM Micrograph images of CCTC single-crystal at various magnifications

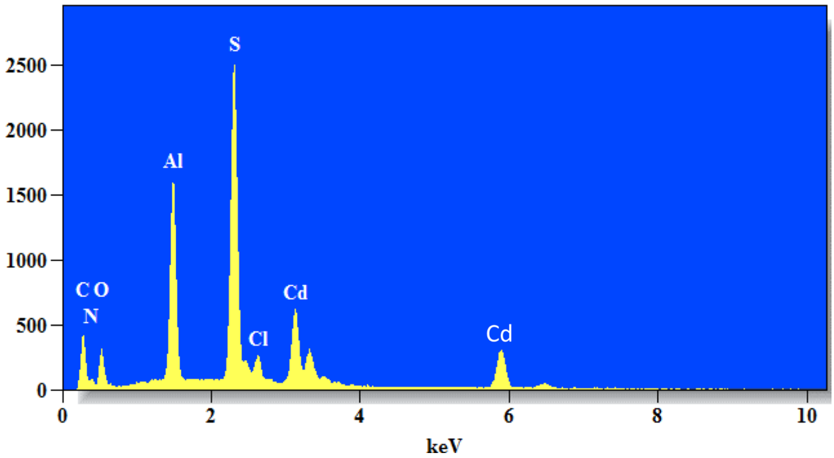

Fig. 8 EDS Spectrum of CCTC

Table 4 Elemental composition of CCTC

Elements	Mass [%]	Atom [%]
C	20.86	38.57
S	22.29	15.44
N	4.38	6.95
Cd	20.71	4.09
Cl	2.61	1.64
Total	70.85	66.69

Table 5 CHNS data of CCTC crystal

Element	N[%]	C [%]	H [%]	S[%]
Experimental	8.459	38.70	6.006	15.179
Calculated	8.13	37.71	5.13	16.33

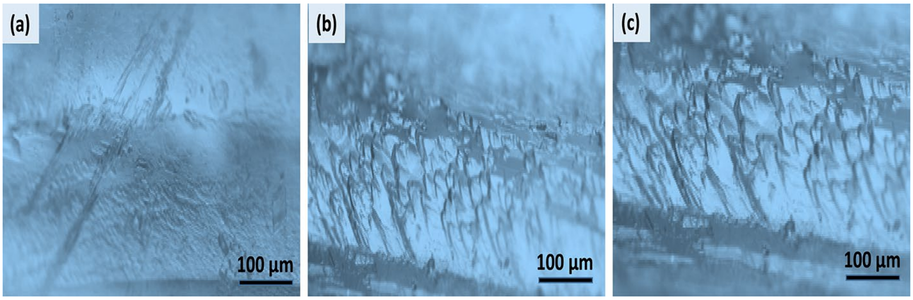

Fig. 9 **a** Etching 5 s, **b** etching 10 s, and **c** After etching 15 s for CCTC single-crystal

3.5 CHNS analysis

Quantitative evidence is provided to support the existence of synthetic compounds with the weight percentages of carbon, hydrogen, sulphur and nitrogen. The experimental and calculated percentages of C, H, S and N are clearly within the experimental errors and very close to each other. In the sample under examination, the calculated sample deviation of the results of the elemental analysis is less than 0.9%. Table 5 provides the CCTC compound theoretical and experimental weight percentages.

3.6 Chemical etching studies

A chemical surface etching test gives information about the structural flaws and reverse growth rate of CCTC crystals when grown. An Olympus high-resolution optical microscope was employed to study the crystal growth surface features. Water, ethanol and methanol were used as etchant agents, and the etching period ranges from 5 to 15 s. The CCTC crystal 5 s of etch pattern is seen in Fig. 9a. The hill rock-shaped etch pattern was seen on the crystal surface after 10 s of the etching process (Fig. 9b). The etch pattern formed in Fig. 9c had a clearly defined size and shape, in this case after etching time increased to 15 s there were no obvious variations in the shape. The calculated etch pit density (EPD) formula is given by

$$\text{Etch pit density} = (\text{Number of etch pits}) / (\text{Area}) \tag{3}$$

An estimated value of EPD calculated as 4×10^6 cm^{-2} which indicates a moderately good crystal quality for the fabrication of optical devices (Ravisankar et al. 2022). The EPD reveals the formation of a hill rock pattern that indicates a 2D growth mechanism.

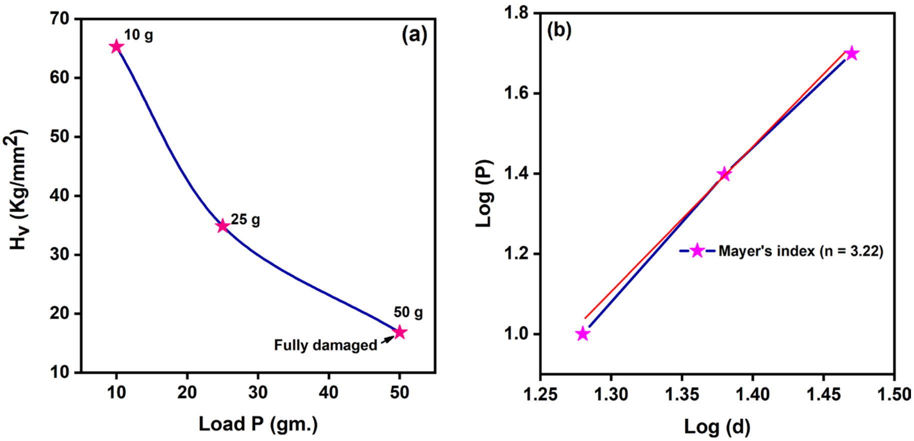

Fig. 10 **a** Vikers hardness Vs Load (P), **b** Log (P) Vs Log (d)

Table 6 Vickers hardness values of CCTC single-crystal

S.No	Load (P) g	Vickers Hardness(Hv) Kg/mm^3
1	10	65.3
2	25	34.86
3	50	16.84

3.7 Mechanical strength studies

Mechanical properties are elastic constant, stiffness and load capacity can be calculated using vickers hardness studies (Sangwal et al. 2000; Vivekanandhan et al. 2018). An economet VH-1MD hardness instrument was attached with a pyramid indenter and maintained a dwell period of 5 s for all loads. The value of hardness (Hv) creating indentation on flat surfaces without any material destruction was studied with applied loads until 10 to 100 g. An indentation (d) seen under microscope view, cracks appear on the surface only on higher loading. Vickers hardness number (H_V) formula (Onitsch et al. 1947)

$$H_v = 1.854\frac{P}{d^2}\left(\frac{Kg}{mm^2}\right) \tag{4}$$

Figure 10a shows Hv as a function of the load P. It is clear that hardness increases as the load increases. By using the straight-line slop method, Fig. 10b shows the log (P) to log (d) ratio (after least square adjustment). Meyer's index number (n), which should be between 1 and 1.6 for hard and above 1.6 for softer ones, is represented by the slope line. In this result study, the calculated 'n' value was 3.22, so the title crystal ideally belongs to soft category material while prepared CCTC matched with other availability organometallic thiocyanate crystals such as BCMTC (3), TMTM (3.07) (Ravisankar et al. 2021a, 2021b, 2021c and Pabitha et al. 2012). Table 6 gives the calculated Hv values.

3.8 Dielectric studies

Two main components of electrical properties: dielectric constant and loss, polarization mechanism of solids can be determined by using dielectric studies (Meena et al. 2018). The measurements were performed using HIOKI 3532–50 LCR meters at room temperature, from 1 Hz to 7 MHz. The calculated dielectric constant (ε_r) formula given by (Miller 1964)

$$\varepsilon_r = \frac{Cpd}{\varepsilon_0 A} \tag{5}$$

where 'C' capacitance (Farads),'d' thickness of the sample (mm) and permittivity ($\varepsilon_0 = 8.854 \times 10^{-12}$ F/m), 'A' area of cross-section (cm). Normally, dielectric constant of the material essentially contribute to electronic, ionic, orientation and space charge polarization (Asokan et al. 2017) depending on frequencies. Figure 11a depicts the ε_r with respect to log frequency and temperature. It is observed that the dielectric constant value is high at lower frequency region. It arises due to the presence of space charge polarization. Furthermore, the space charge polarization will reckon on the purity and perfection of the material. Figure 11b shows the correlation between log frequency and dielectric loss at room temperature. It is observed that the dielectric loss value is high at low frequency region. Materials with high dielectric constant leads to more power dissipation. The characteristic of dielectric constant and loss with lower frequency implies that the CCTC are suitable for electro optic devices.

3.9 Dielectric solid state parameters

In basic solid state electrical properties (SSP), various functions for instance plasma energy ($\hbar\omega_p$), Penn gap (E_P), Fermi energy (E_F) and electronic polarizability (α) were calculated using value of dielectric constant. As norms of the standard procedure, theoretical calculation always depends on the number of valence electrons presented in a given structure.

The density (ρ) is given by (Jackson et al. 1978)

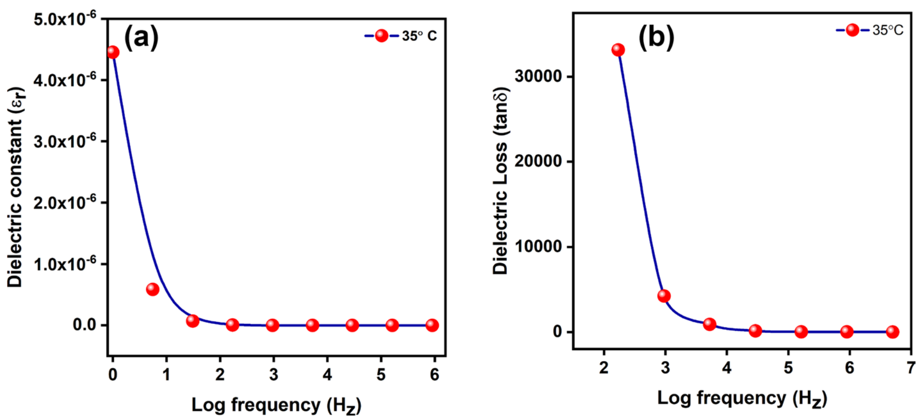

Fig. 11 **a** Dielectric constant (ε′) Vs Log frequency (Hz) **b** Dielectric loss (tan δ) Vs Log frequency (Hz)

$$\rho = \frac{MZ}{N_A V} \tag{6}$$

M = 745.20 g/mol molecular weight ($C_{10}H_{20}O_5$), molecular unit cell (Z = 4), 6.023 10^{23} Avogadro's number (N_A) and unit cell volume (V) 3464.3(2) Å^3. An estimated density (ρ) value confirmed with 1.429 g/cm^3.

The plasma energy ($\hbar\omega_p$) given by (Penn et al. 1962)

$$\hbar\omega_P = 28.8\left(\frac{Z' \times \rho}{M}\right)^{\frac{1}{2}} \tag{7}$$

Total number of valence electrons Z' = [(23 × Z'_C) + (44 × Z'_H) + (1 × Z'_{Cd}) + (4 × Z'_N) + (10 × Z'_O) + (3 × Z'_S) = 236. The values of corresponding elemental valence are C (4), H (1), Cd (2), N (5), O (6), and S (6), for substitutions. Here ε_r is 1 MHz. The relationship between Penn model, E_P and E_F given by (Balarew et al.1984 and Ravindra et al. 1980)

$$E_p = \frac{\hbar\omega_P}{(\varepsilon' - 1)^{\frac{1}{2}}} \tag{8}$$

$$E_F = 0.2948\left(\hbar\omega_P\right)^{\frac{4}{3}} \tag{9}$$

Additionally, we calculated electronic polarizability (α) using the equation

$$\alpha = \left[\frac{\left(\hbar\omega_P\right)^2 S_0}{\left(\hbar\omega_P\right)^2 S_0 + 3E_p^2}\right] \times \frac{M}{\rho} \times 0.396 \times 10^{-24} cm^3 \tag{10}$$

$$S_0 = 1 - \left[\frac{E_p}{4E_F}\right] + \frac{1}{3}\left[\frac{E_p}{4E_F}\right]^2 \tag{11}$$

where S_o is constant, then the electronic polarizability (α) of the CCTC is used to define the Clausius Mossotti (CM) relation, energy band gap (E_g) and coupled dipole method (CDM) (Nijboer, and Renne et al.1968)

$$\alpha = \frac{3M}{4\pi N_A \rho}\left(\frac{\varepsilon' - 1}{\varepsilon' + 2}\right) \tag{12}$$

$$\alpha = \left[1 - \frac{\sqrt{Eg}}{4.06}\right]\left[\frac{M}{\rho}\right] 0.396 \times 10^{-24} cm^3 \tag{13}$$

$$\alpha = \frac{Z' e^2}{m_\rho \omega_o^2} \tag{14}$$

where Z' cumulative number of valence electrons, 1.602 × 10^{-19} electron charge, 9.1 × 10^{-28} mass of electron and 'ω_o' natural frequency ($2\pi f_o$), here 'f_o' is 1 MHz. In SSP results, electronic polarizability is considered as the most important factor at room temperature which is carefully calculated and noted in Table 7.

Table 7 Solid state parameters of CCTC single-crystal

SSP-factors	Calculated values of CCTC crystal
Plasma energy ($\hbar\omega_p$) eV	19.373
Penn gap energy (E_P) eV	0.7440
Fermi energy (E_F) eV	15.187
Electronic polarizability (α) using Penn analysis (cm^3)	2.056×10^{-22}
Electronic polarizability (α) with CM relation (cm^3)	2.058×10^{-22}
Electronic polarizability (α) with E_g (cm^3)	1.260×10^{-22}
Electronic polarizability (α) with CDM (cm^3)	0.716×10^{-22}

3.10 Thermal studies

TG–DTA analysis used to investigate the heating properties of CCTC. The title crystal was performed from room temperature to 900 °C. For this study, NETZSCH STA 449F3 analyzer instrument were used under nitrogen atmosphere at 10 °C per min heating rate. The TG–DTA trace of the CCTC crystal is clearly shown in Fig. 12. The sample's temperature is stable up to 147 °C and was maintained without weight loss between 34 and 147 °C exactly as the suggested water bodies didn't present in synthesized CCTC compounds. The DTA curve also shows three endo-thermic peaks at 194, 320, and 554 °C. Due to the presence of 15-Crown-5, NH_4SCN, and Cd $(SCN)_2$, the first decomposition occurs at 194 °C. The second stage of decomposition occurs at 320 °C indicating a phase change from which the CCTC fragments to the respective metal sulfides, nitrogen gas and cyanogen are released. The third stage occurs at 554 °C which corresponds to the decomposition of the sample. From the above solutions of

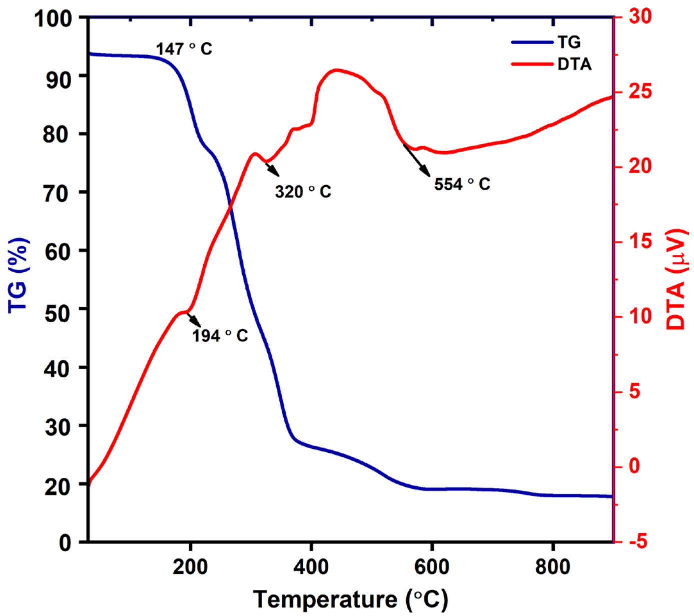

Fig. 12 TG–DTA trace of CCTC

TG–DTA, its obviously confirmed decomposition temperature was at 320 °C. Furthermore, CCTC has better stabilization compared to other thiocyanate complex crystals like CMTG (100 °C), BTC_OC (110 °C) and ATZC (110 °C) (Duan et al. 2002; Senthil Murugan et al. 2008 and Sun et al. 2005).

3.11 Z-scan: third-order non-linear optical studies

The third order NLO properties of the CCTC crystals was studied by using He–Ne laser to generate a Gaussian laser beam source wavelength of 633 nm. The Z-scan experiment setup consisted of a test sample holder (thickness of 1 mm) and convex lens focal length (f = 10 cm) to produce beam waist $\omega_o = 2f\lambda/\pi d$ at the focal point, measured at 5 μm (Sheik-Bahae et al. 1990). An intense laser beam passing through the crystal surface is focused on the focal length of the convex lens, resulting in the transmitted beam being collected by a photodetector using a digital power meter. The whole transmitted beam collected by the detector is called an open aperture (OA) pattern. A transmitted beam pattern passing through the aperture and reaching a detector is called a closed aperture (CA) pattern. The resulting parameters n_2 and β can be determined. Figure 13a and b depict the optical axis (Z axis) of the OA and CA curves, respectively. Rayleigh length (Z_R) is given by

$$Z_R = \frac{\pi\omega_o^2}{\lambda} \tag{15}$$

Rayleigh range (Z_R) calculated value is 0.76 mm, under the condition $Z_R << L$ (Asokan et al. 2017). ΔT_{p-v} is transmittance difference (peak-valley), S is linear aperture transmittance and axis phase shift (ΔΦ) is given by the relations (Shettigar et al. 2007)

$$\Delta\Phi = \frac{\Delta T_{P-V}}{0.406(1-S)^{0.25}} \tag{16}$$

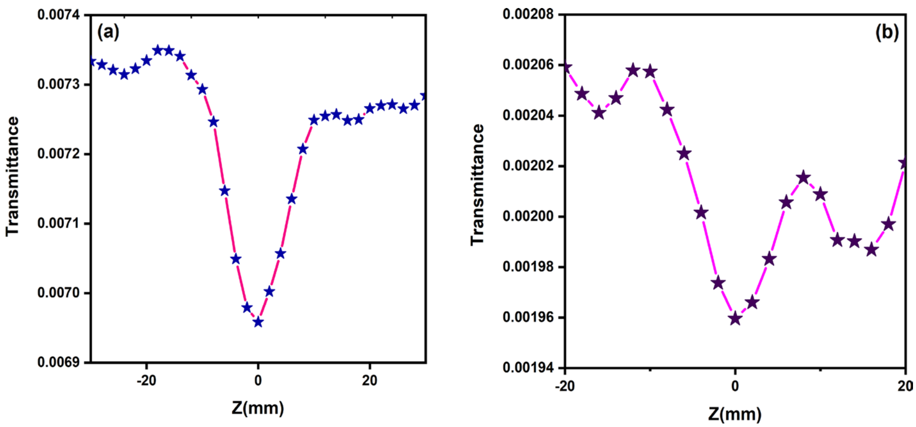

Fig. 13 **a** Open **b** Closed aperture Z-scan patterns of CCTC single-crystal

$$S = 1 - exp\left(\frac{-2r_a^2}{\omega_a^2}\right) \tag{17}$$

where radius of the aperture ($r_a = 3$ mm), aperture beam radius ($\omega_a = 0.5$ cm), an estimated S value is 0.520 and ΔΦ value 0.296. Refractive index (n_2) and absorption (β) relations given by (Van Stryland et al. 1998)

$$n_2 = \frac{\Delta\Phi}{KIoL_{eff}}\left(\frac{m^2}{w}\right) \tag{18}$$

$$\beta = \frac{2\sqrt{2}\Delta\mathrm{T}}{IoL_{eff}}\left(\frac{m}{w}\right) \tag{19}$$

Here, 'K' wave vector (2π/λ), intensity of laser beam (I_o), ΔT peak value of OA and L_{eff} is effective sample thickness, the relationship used to calculate.

$$Leff = \frac{1 - exp(\alpha L)}{L} \tag{20}$$

where 'α' linear absorption coefficient and 'L' sample thickness (1 mm). Real and Imaginary χ3 relations given by (Van Stryland and Sheik-Bahae et al. 1998)

$$R_e\left(\chi^3\right)esu = \frac{10^{-4}\varepsilon_o C^2 n_o^2 n_2}{\pi}\left(\frac{cm^2}{w}\right) \tag{21}$$

$$I_m\left(\chi^3\right)esu = \frac{10^{-2}\varepsilon_o C^2 n_o^2 \lambda\beta}{4\pi^2}\left(\frac{cm}{w}\right) \tag{22}$$

where $\varepsilon_o = 8.854 \times 10^{-12}$ F/m is permittivity, 3×10^8 m/s velocity of light in vacuum (C) and 'n_o' refractive index liner term. The real part added to imaginary part of $\chi.^3$ is given by the relations (Subashini et al. 2011)

$$\chi^3 = \sqrt{\left(R_e\left(\chi^3\right)\right)^2 + \left(I_m\left(\chi^3\right)\right)^2} \tag{23}$$

The second-order hyper polarizability (γ) have been linked to χ^3 (Zhao and Singh et al. 1988).

$$\gamma = \frac{\chi^{(3)}}{N^* f^4} \tag{24}$$

$$N^* = \frac{\rho N_{\mathrm{A}}}{M} \tag{25}$$

where N* represents number of molecules per unit volume. The correction factor (f) and coupling factor (ρ*) is given by

$$f = \frac{(no^2 + 2)}{3} \tag{26}$$

$$\rho^* = \frac{I_m(\chi^3)}{R_e(\chi^3)} \quad (27)$$

Furthermore, χ^3 parameters are OA data that displays reverse saturable absorption (RSA), exhibit that the absorption of the material increases by increasing the laser intensity, making potential candidate for optical applications. The photon energy hν is 1.91 eV lower than the band gap energy of 2.5 eV. Once the photon energy incident on a CCTC crystal, it absorbs two photons of energy hν to reach a higher energy state, once the ground state electrons get depleted, the absorption will starts from the first exited state, this type of absorption is called RSA. The CA pattern exhibit pre-focal peak and post-focal valley, indicating self-defocusing (SDF) nature of the material. It shows a negative refractive index of the material. For self-focusing to occur beam intensity should reach a certain threshold, a beam with less power will undergo self-defocusing irrespective of the material. A beam with less power will not undergo self-focusing even it is focused tight therefore we get self-defocusing. The estimated third-order NLO values $n_2 = 2.516 \times 10^{-9} cm^2W^{-1}$ and $\beta = 0.954 \times 10^{-5} cmW^{-1}$, respectively. Therefore, the calculated χ^3 value of CCTC crystal was 2.577×10^{-5} esu also second-order hyperpolarizability (γ) value 1.43×10^{-27} esu and coupling factor (ρ*) is 1.914. However, hyperpolarizability is associated with the d-d transition at low energy with the electron delocalization system interacting due to increased charge transfer of the dipole moment. The above results reveal the title compound used for frequency tripling and optical switching applications. The organometallic thiocyanate family MCCTC (Ramesh et al. 2020) crystal compared to CCTC have a greater value of χ^3 summarized in Table 8.

4 Conclusion

The title compound of CCTC was synthesized by using the slow evaporation method at ambient temperature. The SXRD pattern confirms, the monoclinic structure and centrosymmetric space group $P2_{1/n}$. The sample cut-off was found to be 271 nm, with a band gap of 2.5 eV (Tauc's plot). The presence of C-N stretching molecular vibrations of the thiocyanate ligand (2064 cm^{-1}) and metal-nitrogen vibrations (468 and 821 cm^{-1}) was confirmed by the FTIR spectrum. An existence of crack-free nature of the surface, randomly oriented needle shape structures were confirmed through HR-SEM analysis. The chemical composition of the grown crystal formula [C_{23} H_{44} Cd N_4 O_{10} S_3] is well-matched with the EDS spectrum and CHNS analysis. Etching studies reveals that the crystal surface pattern shows a hill rock shape layer and the calculated EPD value is 4×10^6 cm^{-2}. The sample stability was confirmed up to 147 °C. The dielectric constant (ε_r) has a higher value in the low-frequency region and lower value in the high-frequency region and is active in space charge polarization. Additionally, the solid state parameters are calculated theoretically. The hardness testing reveals the material type is soft (n = 3.22). Furthermore, OA and CA data reveal RSA and SDF natures. The calculated values are non-linear absorption (β) $0.954 \times 10^{-5} cmW^{-1}$, refractive index $(n_2) = 2.516 \times 10^{-9} cm^2W^{-1}$ and third-order susceptibility $(\chi^3) = 2.577 \times 10^{-5}$esu, respectively. The optical properties of the title compound used for frequency tripling and optical limiting applications.

Table 8 Z-scan measurement details and the various parameters of the CCTC single-crystal compared to MCCTC

Z-scan parameters	CCTC	MCCTC
Laser type	He–Ne laser	He–Ne laser
Wavelength of laser (nm)	633	633
Focal length (f) cm	20	–
Laser beam-diameter (cm)	0.1	–
Sample thickness (cm)	0.1	–
Aperture radius (mm)	3.3	–
Intensity of the laser (KW/cm^2)	25	–
Optical path distance (mm)	1	–
Beam waist (ω_o) µm	12.04	–
Rayleigh length (Z_R) mm	0.76	–
Effective thickness (L_{eff}) mm	0.47	
Refractive index n_2 (cm^2/W)	2.416×10^{-9}	8.57×10^{-13}
Absorption coefficient β (cm/W)	0.954×10^{-5}	8.14×10^{-6}
Real part of TONLO [R_e (χ^3)] (cm^2/W)	25.290×10^{-6}	–
Imaginary part of TONLO [I_m (χ^3)] (cm/W)	4.834×10^{-7}	–
TONLO (χ^3) esu	2.577×10^{-5}	2.49×10^{-9}
Second order molecular hyper polarizability (γ) esu	1.43×10^{-27}	–
Number of molecules per cm^3 (N*)	$11.54 \times 10^{+20}$	–
Coupling factor (ρ*)	1.914	–

Acknowledgements The authors thank the management of the Sathyabama institute of science and technology, Chennai, for providing excellent research facilities. The authors are very much thankful to SAIF, IIT Madras, for providing single crystal XRD studies.

Author contributions Both the authors contributed to the study conception and design. Material preparation, data collection and analysis were performed by S. Ramkumar and P. Malliga. The first draft of the manuscript was written by S. Ramkumar and both authors commented on previous versions of the manuscript. All authors read and approved the final manuscript.

Funding The authors declare that no funds, grands, or other support were receive during the preparation of this manuscript.

Availability of data and materials The data that support the findings of this study are available from the corresponding author upon reasonable request.

Declarations

Conflict of interest The authors declare that they have no conflict of interest.

Ethical approval Not applicable.

References

Ashok Hegde, T., Dutta, A., Vinitha, G.: χ^3 measurement and optical limiting behavior of novel semi-organic cadmium mercury thiocyanate crystal by Z-scan technique: CMTC. Appl. Phy. A **124**, 1–10 (2018)

Asokan, P., Kalainathan, S.: Bulk crystal growth, optical, electrical, thermal, and third order NLO properties of 2-[4-(Diethylamino)benzylidene]malononitrile (DEBM) single crystal. J. Phys. Chem. C **121**(40), 22384–22395 (2017)

Balarew, C., Duhlew, R.: Application of the hard and soft acids and bases concept to explain ligand coordination in double structures. J. Solid State Chem. **551**, 1–6 (1984)

Bruker APEX2 and SAINT, Bruker AXS Inc., Madison, Wisconsin, USA, (2008).

Cliffe, M.J., Keyzer, E.N., Dunstan, M.T., Ahmad, S., Devolder, M.F.L., Deschler, F., Morris, A.J., Grey, C.P.: Strongly colored thiocyanate frameworks with perovskite-analogue structures. Chem. Sci. **10**(3), 793–801 (2019)

Duan, X.L., Yuan, D.R., Wang, X.Q., Cheng, X.F., Yang, Z.H., Guo, S.Y., Sun, H.Q., Xu, D., Lu, M.K.: Preparation and characterization of nonlinear optical crystal materials: cadmium mercury thiocyanate (CMTG) and its lewis base adducts. Cryst. Res. Technol. **37**, 446–455 (2002)

Jackson, J.D.: ClassicalElectrodynamics, 3rd edn. Wiley Eastern Limited, New Delhi (1978)

Johnson, J., Srineevasan, R., Sivavishnu, D.: Process development and characterization of centrosymmetric semiorganic nonlinear optical crystal: 4-dimethylaminopyridine potassium chloride. Physica B Phys. Condens. Matter. **538**, 199–206 (2018). https://doi.org/10.1016/j.physb.2018.03.038

Kamalesh, T., Karuppasamy, P., Senthilkumar, C., Senthil Pandian, M., Ramasamy, P., Sunil, V.: Growth, structural, Hirshfeld surface, optical, laser damage threshold, dielectric and chemical etching analysis of 4-dimethylaminopyridinium 4-nitrophenolate 4-nitrophenol (DMAPNP) single crystal. J. Mater. Sci. Mater. Electron. **31**, 373–386 (2020)

Karuppasamy, P., Sivasubramani, V., Senthil Pandian, M., Ramasamy, P.: Growth and characterization of semi-organic third order nonlinear optical (NLO) potassium 3, 5- crystals. RSC Adv. **6**, 109105–109123 (2016)

Mahendiran, D., Vinitha, G., Shobana, S., Viswanathan, V., Velmurugan, D., Rahiman, A.K.: Theoreticalphotophysical and biological investigations of an organic charge transfer compound2-aminobenzimidazolium-2-oxyisoindolate-1, 3-dione-2-hydroxyisoindoline-1, 3-Dione. RSC Adv. **6**, 60336–60348 (2016)

Meena, M., Mahadevan, C.K.: Growth and electrical characterization of L-arginine added KDP and ADP single crystals. Cryst. Res. Technol. **43**(2), 166–172 (2008)

Miller, R.: Optical second harmonic generation in pezoelectic crystals. Appl. Phys. Lett. **5**, 17–19 (1964)

Nijboer, B.R.A., Renne, M.J.: Microscopic derivation of macroscopic Vander waals forces. Chem. Phys. Lett. **2**, 35–38 (1968)

Onitsch, E.M.: Systematic metallographic and mineralogic structures. Mikroscopia **2**, 131–151 (1947)

Pabitha, G., Dhanasekaran, R.: Investigation on the crystal growth and characterization of an organometallic nonlinear optical crystal Tetrathiourea mercury tetrathiocynate manganite. Mater. Sci. Eng. B **177**, 1149–1155 (2012)

Parol, V., Prabhu, A.N., Taher, M.A., Naraharisetty, S.R.G., Lokanath, N.K., Upadhyaya, V.: A third-order nonlinear optical single crystal of 3, 4-dimethoxy-substituted chalcone derivative with high laser damage threshold value: a potential material for optical power limiting. J. Mater. Sci. Mater. Electron. **31**, 9133–9150 (2020)

Penn, D.R.: Wave number dependent dielectrics function of semiconductors. Phys. Rev. **128**, 2093–2097 (1962)

Raghavan, C.M., Bhaskaran, A., Sankar, R., Jayavel, R.: Studies on the growth, structural, optical, thermal and electrical properties of nonlinear optical CMTG crystal. Current Appl. Phy. **10**, 479–483 (2010)

Rajarajan, K., Sendil Kumar, K.: Spectroscopic, optical, thermal, and AC conductivity studies on semi-organic nonlinear optical crystal: AMCTC. J. Therm. Anal. Calorium **112**, 1297–1302 (2013)

Ramesh, V., Rajarajan, K.: Crystal growth and characterization of a novel inorganic-organic hybrid NLO crystal: (NH_4) [Cd $(NCS)_3$].$C_{12}H_{24}O_6$]. Appl. Phys. B **113**, 1–6 (2013)

Ramesh, V., Sendil Kumar, K., Subashini, A., Shihabuddeen, A., Jaganathan, K.: Experimental investigations on the synthesis, growth and characterization of MCCTC single crystal. AIP Conf. Proc. **1447**, 1287–1288 (2012)

Ramesh, V., Gunasekaran, B., Suresh, P., Sundaravadivel, E., Showrilu, K., Rajarajan, K.: Crystal growth, surface morphology, mechanical and thermal properties of UV-nonlinear optical crystal: Mercury cadmium chloride thiocyanate (MCCTC) single crystal. Mater. Sci. Eng. **872**, 1–8 (2020)

Ravindra, N.M., Srivastava, V.K.: Electronic polarizability as a function of the penn gap in semiconductors. J. Infrared Phys. **20**, 67–69 (1980)

Ravisankar, V., Ramesh, V., Krishna Mohan, M., Gunasekarana, B., Sabari Girisun, T., Dhanusha, A.: Synthesis, growth, structural and physicochemical properties of a novel linear and nonlinear UV-optical single-crystal for photonic applications: [Ba $(C_{14}H_{20}O_5)_2$Co $(SCN)_4$]. ECS J. Solid State Sci. Tech. **10**, 1–13 (2021a)

Ravisankar, V., Ramesh, V., Krishnamohan, M., Gunasekaran, B., Sabari Girisun, T.: Bis(benzo-15-crown-5-j5O)bariumtetraki(isothiocyanatokN)cobaltate(II). IUCrData **6**, 2414–3146 (2021b)

Ravisankar, V., Ramesh, V., Sridevi, D.V., Gunasekaran, B., Sabari Girisun, T.C.: Synthesis, growth, structural, physicochemical, linear and nonlinear optical properties of new hybrid $[(Ba(C_{10}H_{20}O_5)_2$ (Mn $(SCN)_4)]$ single crystal. Appl. Phy. A **127**, 1–15 (2021c)

Ravisankar, V., Ramesh, V., Gunasekarana, B., Sabari Girisun, T.: Synthesis, growth, structural, physicochemical, linear, and nonlinear optical properties of new hybrid $[2(C_{10}H_{20}O_5)$ Ba] [Co $(SCN)_4]$ single crystal. J. Mater. Sci. Mater. Electron. **33**, 9380–9394 (2022)

Rhoufal, F., Laachir, A., Guesmi, S., Jouffret, L., Sergent, N., Obbade, S., Akkurt, M., Bentiss, F.: New cobalt(II) and copper(II) thiocyanate complexes of 2,5-bis(pyridin-2-yl)-1,3,4-oxadiazole ligand. Chem. Select **4**, 7773–7783 (2019)

Robert, R., Justin Raj, C., Krishnan, S., Jerome Das, S.: Growth, theoretical and optical studies on potassium dihydrogen phosphate (KDP) single crystals by modified Sankaranarayanan-Ramasamy (MSR) method. Physica B **405**, 20–24 (2010)

Sangwal, K.: On the reverse indentation size effect and microhardness measurement of solids. Mater. Chem. Phys. **63**, 145–152 (2000)

Saravanan, N., Chidambaram, V., Ravisankar, V.: Growth and characterization of novel semi organic nonlinear optical urea lead acetate single crystal by solution growth technique. J. Mater. Sci. Mater. Electron. **29**, 5009–5013 (2018)

Senthil, K., Kalainathan, S., Ruban Kumar, A., Aravindan, P.G.: Investigation of synthesis, crystal structure and third order NLO properties of new stilbazolium derivative crystal: a promising material for nonlinear optical devices. RSC Adv. **4**, 56112–56127 (2014)

Senthil Murugan, G., Balamurugan, N., Ramasamy, P.: Growth and characterization of a new metal-organic crystal: bis-thiourea cobalt chloride (BTCoC). Mater. Lett. **62**, 3087–3090 (2008)

Sheik-Bahae, M., Said, A.A.: Sensitive measurement of optical nonlinearities using a single beam. J. Quantum. Electron. **26**, 760–769 (1990)

Sheldrick, G.M.: SADABS program for area detector absorption correction. University of Gottingen, Germany (1996)

Sheldrick, G.M.: A short history of SHELX. Acta Cryst. **A64**, 112–122 (2008)

Shettigar, S., Umesh, G., Chandrasekharan, K., Kalluraya, B.: Third-order nonlinear optical properties and two-photon absorption in newly synthesized phenylsydnone doped polymer. Synth. Metals **157**(15), 142–146 (2007)

Subashini, A., Kumaravel, R., Leela, S., Evans, H.S., Sastikumar, D., Ramamurthi, K.: Synthesis, growth and characterization of 4-bromo-4'chloro benzylidene aniline–a third order nonlinear optical material. Spectrochim. Acta Part A Mol. Biomol. Spectrosc. **78**, 935–941 (2011)

Sun, H.Q., Yuan, D.R., Wang, X.Q., Cheng, X.F., Gong, C.R., Zhou, M., Xu, H.Y., Wei, X.C., Luan, C.N., Pan, D.Y., Li, Z.F.: A novel metalorganic coordination complex crystal: tri-allylthiourea zinc chloride (ATZC). Cryst. Res. Technol. **40**, 882–886 (2005)

Suresh, T., Vetrivel, S., Gopinath, S., Vinoth, E.: A new NLO material L-Asparagine thiocynate for opto electronic applications: LATC. Chin. J. Phys. **18**, 1–9 (2018)

Van Stryland, E.W., Sheik-Bahae, M.: Z-scan measurements of optical nonlinearities, characterization techniques and tabulations for organic nonlinear materials. Org. Nonlinear Mater. **18**, 655–692 (1998)

Vijayalakshmi, A., Vidyavathy, B., Vinitha, G.: "Crystal structure, growth and nonlinear optical studies ofsonicotinamide p-nitrophenol: a new organic crystal for optical limiting applications. J. Cryst. Growth **448**, 82–88 (2016)

Vivekanandhan, R., Raju, K., S. Sahaya Jude Dhas, V. Chithambaram,: Investigation on novel nonlinear optical L-threonine calcium chloride single crystal grown by solution growth technique. Int. J. Appl. Eng. Res. **13**, 13454–13459 (2018)

Yuanet, D.R.: Growth of cadmium mercury thiocyanate single crystal for laser diode frequency doubling. J. Cryst. Growth **186**, 240–244 (1988)

Zhao, M.T., Singh, B.P., Prasad, P.N.: A systematic study of polarizability and microscopic third-order optical nonlinearity in thiophene oligomers. J. Chem. Phys. **89**, 5535–5541 (1988)

Publisher's Note Springer Nature remains neutral with regard to jurisdictional claims in published maps and institutional affiliations.